

Further success of the colour dipole model

J.R. Forshaw¹, R. Sandapen² and G. Shaw¹

¹*School of Physics & Astronomy, University of Manchester,
Oxford Road, Manchester M13 9PL, U.K.*

²*Département de Physique et d'Astronomie, Université de Moncton, Moncton, N-B.
E1A 3E9. Canada.*
forshaw@mail.cern.ch

ABSTRACT: We confront a very wide body of HERA diffractive electroproduction data with the predictions of the colour dipole model. We focus upon three different parameterisations of the dipole scattering cross-section and find good agreement for all observables. There can be no doubting the success of the dipole scattering approach and more precise observations are needed in order to expose its limitations.

Contents

1. Introduction	1
2. The dipole cross-section	3
2.1 The FS04 Regge model	3
2.2 The FS04 Saturation model	4
2.3 The CGC saturation model	4
3. Exclusive processes	5
3.1 Deeply virtual Compton scattering	6
4. J/Ψ and the charm structure function	7
4.1 The charm structure function	7
4.2 J/Ψ wavefunctions	9
4.3 J/Ψ electroproduction	12
5. Diffractive deep inelastic scattering (DDIS)	18
6. Conclusion	23

1. Introduction

In the colour dipole model [1, 2], the forward amplitude for virtual Compton scattering is assumed to be dominated by the mechanism illustrated in Fig.1 in which the photon fluctuates into a $q\bar{q}$ pair of fixed transverse separation r and the quark carries a fraction z of the incoming photon light-cone energy. Using the Optical Theorem, this leads to

$$\sigma_{\gamma^*p}^{L,T} = \int dz d^2r |\Psi_{\gamma}^{L,T}(r, z, Q^2)|^2 \sigma(s^*, r) \quad (1.1)$$

for the total virtual photon-proton cross-section, where $\Psi_{\gamma}^{L,T}$ are the appropriate spin-averaged light-cone wavefunctions of the photon and $\sigma(s^*, r)$ is the dipole cross-section. The dipole cross-section is usually assumed to be independent of z , and is parameterised in terms of an energy variable s^* which depends upon the model.

Thus using Eq.(1.1) we are able to compute the deep inelastic structure function $F_2(x, Q^2)$. The power of the dipole model formulation lies in the fact that the same dipole cross-section $\sigma(s^*, r)$ appears in a variety of other observables which involve the scattering of a real or virtual photon off a hadronic (or nuclear) target at high centre-of-mass (CM) energy. The largeness of the CM energy guarantees the factorization of scattering amplitudes into a product of wavefunctions and a universal dipole cross-section. In this paper we

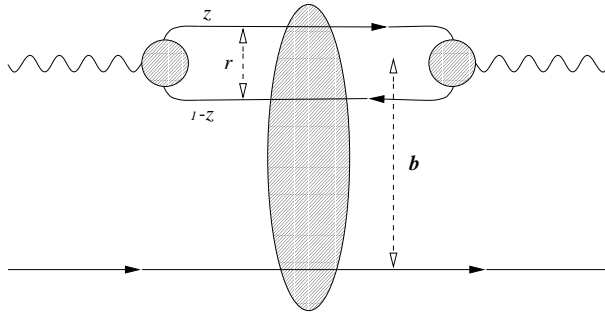


Figure 1: The colour dipole model for elastic Compton scattering $\gamma^*p \rightarrow \gamma^*p$.

wish to test the universality of the dipole cross-section using a wide range of high quality data collected at the HERA ep collider. Moreover, we also wish to examine the extent to which data are able to inform us of the role, if any, played by non-linear saturation dynamics.

Specifically, we shall consider three particular parameterisations of the dipole cross-section which have been presented in the literature and which will be discussed in more detail below. All three have been constrained by fitting only to the HERA data on $F_2(x, Q^2)$ and so they can be used to make genuine predictions for other observables. In this paper we will compare those predictions to data on the charm structure function $F_2^c(x, Q^2)$, the cross-section for Deeply Virtual Compton Scattering (DVCS), the cross-section for diffractive J/Ψ production and the diffractive structure function $F_2^{D(3)}$.

In the first instance our results confirm the validity of the dipole model: it does make sense to speak of a universal dipole cross-section which is able to account for both soft and hard diffraction in a wide variety of photo-processes. We also attempt to ascertain the extent to which the new data are able to discriminate between the predictions of the three dipole models we use. These models can perhaps best be described as parameterisations which incorporate certain general theoretical ideas and can be viewed as providing an indication of the uncertainties remaining in the dipole cross-section once the precise structure function data have been accounted for. Unfortunately we shall find that the new data are not quite precise enough to discriminate between the models or to add any significant evidence for saturation beyond that already present in the F_2 data. We do however find that in diffractive photo/electro-production progress is hindered by the lack of a precise enough measurement of the forward slope parameter B which determines the t -dependence of the final state proton. We take this parameter from data and its error translates into an uncertainty on the normalisation of the predicted cross-sections. A more precise measurement of this quantity would provide a significant additional constraint.

It is clear that having extracted the dipole cross-section from data, one would hope eventually to explain the result using QCD. Unfortunately, while QCD in its present state of development is able to suggest qualitative features of the dipole cross-section, more quantitative predictions are not possible without severe approximations. To remedy this situation is a challenge which lies beyond the scope of this paper.

2. The dipole cross-section

We now turn to the three different models used to describe the dipole cross-section. Before doing so however, we shall first discuss our choice of photon wavefunction. For small r , the light-cone photon wavefunctions are given by the tree level QED expressions [1]

$$|\Psi_\gamma^L(r, z, Q^2)|^2 = \frac{6}{\pi^2} \alpha_{\text{em}} \sum_{f=1}^{n_f} e_f^2 Q^2 z^2 (1-z)^2 K_0^2(\epsilon r) \quad (2.1)$$

$$|\Psi_\gamma^T(r, z, Q^2)|^2 = \frac{3}{2\pi^2} \alpha_{\text{em}} \sum_{f=1}^{n_f} e_f^2 \{ [z^2 + (1-z)^2] \epsilon^2 K_1^2(\epsilon r) + m_f^2 K_0^2(\epsilon r) \} \quad (2.2)$$

where

$$\epsilon^2 = z(1-z)Q^2 + m_f^2 . \quad (2.3)$$

Here $K_0(x)$ and $K_1(x) = -\partial_x K_0(x)$ are modified Bessel functions and the sum is over all $n_f = 4$ quark flavours f . These wavefunctions decay exponentially at large r , with typical r -values of order Q^{-1} at large Q^2 and of order m_f^{-1} at $Q^2 = 0$. However for large dipoles $r \gtrsim 1$ fm, which are important at low Q^2 , a perturbative treatment is not really appropriate. In this region some authors [3] modify the perturbative wavefunction by an enhancement factor motivated by generalised vector dominance (GVD) ideas [4, 5, 6], while others [7] achieve a similar but broader enhancement by varying the quark mass¹. In practice [9], the difference between these two approaches only becomes important when analysing the precise real photoabsorption data from fixed-target experiments [10]. Since we will not consider these data here, we will adopt the simpler practise of using a perturbative wavefunction at all r -values, and adjusting the quark mass to fit the data.

Turning now to the dipole cross-section, all three models are consistent with the physics of colour transparency for small dipoles and exhibit soft hadronic behaviour for large dipoles. As stated above, the model parameters are determined by fitting only to the DIS structure function data. The resulting dipole cross-sections can then be used to make genuine predictions for other reactions. Since the details of all three models have been published elsewhere, we shall here summarise their properties only rather briefly.

2.1 The FS04 Regge model

This simple model [9] combines colour transparency for small dipoles $r < r_0$ with ‘‘soft pomeron’’ behaviour for large dipoles $r > r_1$ by assuming

$$\begin{aligned} \sigma(x_m, r) &= A_H r^2 x_m^{-\lambda_H} \quad \text{for } r < r_0 \quad \text{and} \\ &= A_S x_m^{-\lambda_S} \quad \text{for } r > r_1, \end{aligned} \quad (2.4)$$

where

$$x_m = \frac{Q^2}{Q^2 + W^2} \left(1 + \frac{4m_f^2}{Q^2} \right). \quad (2.5)$$

¹For a fuller discussion of these points see [8].

For light quark dipoles, the quark mass m_f is a parameter in the fit, whilst for charm quark dipoles the mass is fixed at 1.4 GeV. In the intermediate region $r_0 \leq r \leq r_1$, the dipole cross-section is given by interpolating linearly between the two forms of Eq.(2.4).

If the boundary parameters r_0 and r_1 are kept constant then this parameterisation reduces to a sum of two powers, as might be predicted in a two pomeron approach, and can be thought of as an update of the original FKS Regge model [3] to accommodate the latest data. It is plainly unsaturated, in that the dipole cross-section obtained at small r -values and fixed Q^2 grows rapidly with increasing s (or equivalently with decreasing x) without damping of any kind.

2.2 The FS04 Saturation model

Saturation can be introduced into the above model by adopting a method previously utilised in [11]. Instead of taking r_0 to be constant, it is fixed to be the value at which the hard component is some specified fraction of the soft component, i.e.

$$\sigma(x_m, r_0)/\sigma(x_m, r_1) = f \tag{2.6}$$

and f instead of r_0 is treated as a parameter in the fit. This introduces no new parameters compared to the Regge model. However, the scale r_0 now moves to lower values as x decreases, and the rapid growth of the dipole cross-section at a fixed, small value of r begins to be damped as soon as r_0 becomes smaller than r . In this sense we model saturation, albeit crudely, with r_0 the saturation radius.

2.3 The CGC saturation model

In addition we shall consider the CGC dipole model originally presented by Iancu, Itakura and Munier [12]. This model aims to include the main features of the ‘‘Colour Glass Condensate’’ regime, and can be thought of as a more sophisticated version of the original ‘‘Saturation Model’’ of Golec-Biernat and Wüsthoff [7]. Since the original Iancu et al dipole cross-section was obtained after a three flavour fit to the DIS data it is not well suited to making predictions for processes involving charm quarks. Consequently, we instead use a new four-flavour CGC fit due to Kowalski, Motyka and Watt [13].

The parameters of the FS04 models were determined by fitting the recent ZEUS F_2 data [14] in the kinematic range

$$0.045 \text{ GeV}^2 < Q^2 < 45 \text{ GeV}^2 \quad x \leq 0.01 \tag{2.7}$$

whilst the CGC fit of [13] is to data with $Q^2 > 0.25 \text{ GeV}^2$ (the other limits are as for FS04). The corresponding H1 data [15] could also be used, but it would then be necessary to float the relative normalisation of the two data sets. We do not do this since the ZEUS data alone suffice. The resulting parameter values are tabulated in the original papers; we do not reproduce them here, but confine ourselves to some general comments.

Both the FS04 saturation and the CGC models gave excellent fits to the F_2 data, while the FS04 Regge fit was not satisfactory, suggesting that saturation may be required to fit the data [9].² However this evidence for saturation depends upon using low- Q^2 data and disappears if the data are restricted to $Q^2 > 2 \text{ GeV}^2$, whereupon excellent fits can be obtained in all three models.

We use the CGC fit with $\sigma_0 = 35.7 \text{ mb}$ presented in Table 5 of [13] and note that although the fit is to data with $Q^2 > 0.25 \text{ GeV}^2$ the fit is actually very good all the way down to $Q^2 = 0.045 \text{ GeV}^2$.

At this point we have three well-determined parameterisations of the colour dipole cross-section. These can be used to yield predictions for other processes. In the next sections we shall take a look at Deeply Virtual Compton Scattering (DVCS), the charm structure function F_2^c , exclusive J/Ψ production and the diffractive structure function $F_2^{D(3)}$. We always choose to show the Regge fit, even though it does not fit the F_2 data particularly well, in order to indicate the discriminatory power of the data. We stress that in all cases, the photon wavefunctions and dipole cross-sections are precisely those determined from the fits to F_2 data, without any adjustment of parameters.

3. Exclusive processes

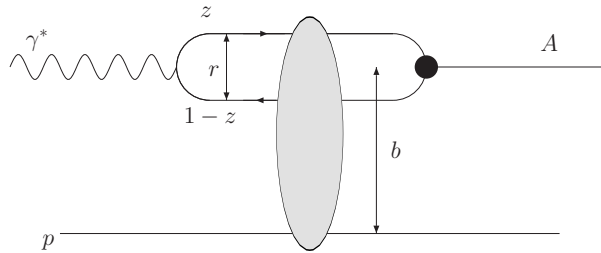


Figure 2: The colour dipole model for the exclusive reactions $\gamma^* p \rightarrow A p$.

We are interested in the exclusive processes

$$\gamma^* + p \rightarrow A + p \quad A = \gamma, \rho, J/\Psi, \dots \quad (3.1)$$

In the dipole model they occur via the mechanism of Fig.2 and are described by amplitudes which satisfy

$$\text{Im}A_\lambda(s, t = 0) = s \sum_{h, \bar{h}} \int d^2z d^2r \Psi_{h, \bar{h}}^A(r, z) \Psi_{h, \bar{h}}^{\gamma, \lambda}(r, z, Q^2) \sigma(s^*, r) \quad (3.2)$$

where $\lambda = L, T$ for longitudinal and transverse photons respectively, h and \bar{h} are the quark and antiquark helicities and $\Psi_{h, \bar{h}}^A(r, z)$ is the light-cone wavefunction of the particle A . The

²The FS04 saturation fit has a $\chi^2 = 155$ for the 156 data points we consider. For the same data, the CGC model has $\chi^2 = 160$ and the FS04 Regge fit has $\chi^2 = 428$.

forward differential cross-section is then given by

$$\left. \frac{d\sigma}{dt} \right|_{t=0} = \frac{1}{16\pi s^2} |A_\lambda(s, t=0)|^2 (1 + \beta^2), \quad (3.3)$$

where the correction from the real part of the amplitude

$$\beta = \frac{\text{Re}A_\lambda(s, t=0)}{\text{Im}A_\lambda(s, t=0)}$$

can be estimated using dispersion techniques. Predictions for the measured total cross-sections are then obtained by assuming an exponential t -distribution and integrating over t to obtain

$$\sigma_{L,T}(\gamma^* p \rightarrow Ap) = \frac{1}{B} \left. \frac{d\sigma^{T,L}}{dt} \right|_{t=0}, \quad (3.4)$$

where the value of the slope parameter B is taken from experiment. We refer to [13, 16] for models which attempt a more sophisticated treatment of the dependence upon the momentum transfer, t .

The exclusive processes we consider in this paper are DVCS and J/Ψ production. Light meson production was studied in our previous paper [17] where we found that the dipole model predictions generally agree well with the data modulo a rather strong dependence upon the meson wavefunction. For an alternative investigation of the link which exists between low x DIS and exclusive processes at high energies we refer to [18].

3.1 Deeply virtual Compton scattering

In deeply virtual Compton scattering

$$\gamma^* + p \rightarrow \gamma + p, \quad (3.5)$$

the final state particle is a real photon and dipole models provide predictions for the imaginary part of the forward amplitude with no adjustable parameters beyond those used to describe DIS. To calculate the forward cross-section a correction for the contribution of the real part of the amplitude has to be included. This correction was estimated in [19] and found to be less than $\approx 10\%$ and of a similar size in different dipole models. Here we shall estimate the correction using the FS04 Regge model, where the real part is given by the Regge signature factors. Predictions for the measured total cross-sections are then obtained using Eq.(3.4) where the value of the slope parameter B is taken from experiment.

The predictions of all three models are compared with the H1 data [20] in Fig.3 and Fig.4 and with the ZEUS data [21] in Fig.5 and Fig.6.³ For the H1 data we use a fixed value $B = 6.02 \text{ GeV}^{-2}$ for the slope parameter which is in accord with the H1 measurement of $B = 6.02 \pm 0.35 \pm 0.39$. For the ZEUS data we take $B = 4 \text{ GeV}^{-2}$ which is compatible with their data. Bearing in mind this normalisation uncertainty, the agreement is good for all three models, although significant differences between the models appear when the predictions are extrapolated to high enough energies, as one would expect.

³Note that throughout this paper the curves labelled ‘FS04 no sat’ correspond to the predictions of the FS04 Regge model.

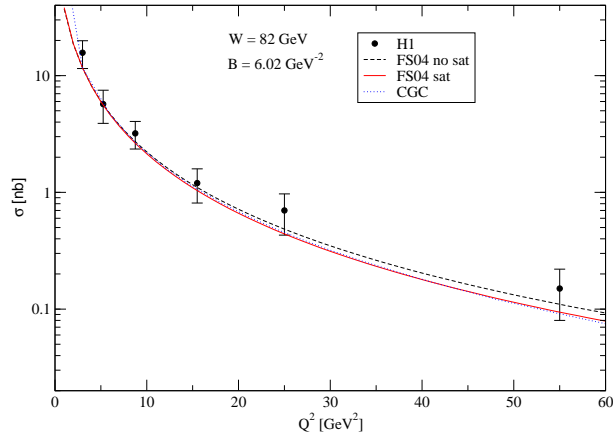


Figure 3: Comparison of the H1 DVCS data [20] with the predictions of the three models discussed in the text: Q^2 dependence at $W = 82$ GeV.

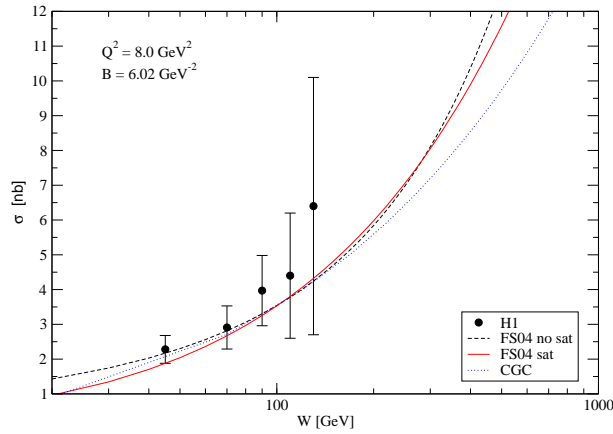


Figure 4: Comparison of the H1 DVCS data [20] with the predictions of the three models discussed in the text: W dependence at $Q^2 = 8.0$ GeV².

4. J/Ψ and the charm structure function

We now move on to the predictions for the charm structure function and for exclusive J/Ψ production

$$\gamma^* + p \rightarrow J/\Psi + p \quad . \quad (4.1)$$

All three models assume a charm mass of $m_C = 1.4$ GeV when fitting the F_2 data. Since the exclusive process is rather more sensitive to the charm mass we will allow m_c to vary a little without adjusting the dipole cross-section. This is permissible for small enough variations.

4.1 The charm structure function

We begin by discussing the charm structure function $F_2^c(x, Q^2)$, since the results are independent of the vexed question of the vector meson wavefunction. The charm structure

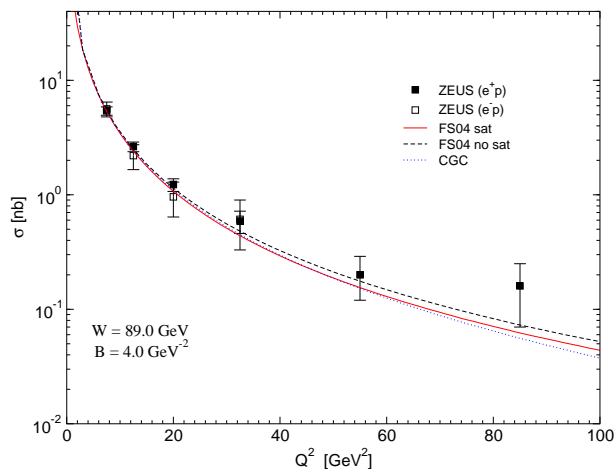


Figure 5: Comparison of the ZEUS DVCS data [21] with the predictions of the three models discussed in the text: Q^2 dependence at $W = 89$ GeV.

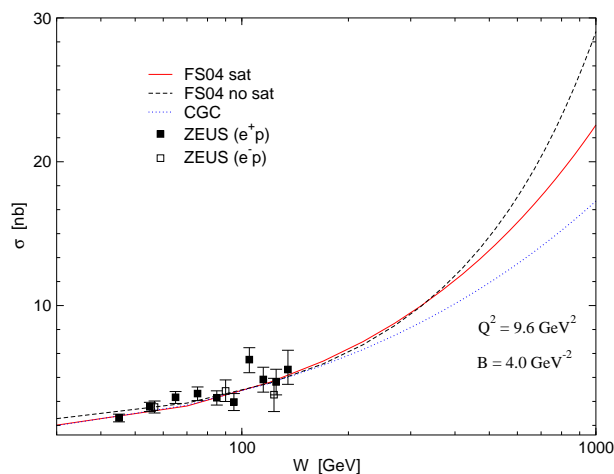


Figure 6: Comparison of the ZEUS DVCS data [21] with the predictions of the three models discussed in the text: W dependence at $Q^2 = 9.6$ GeV².

function is given by

$$F_2^c(x, Q^2) = \frac{Q^2}{4\pi^2\alpha_{\text{em}}} (\sigma_{\gamma^*p}^L + \sigma_{\gamma^*p}^T)$$

where in calculating the total virtual photon-proton cross-sections using Eq.(1.1), only the charm component of the light-cone wavefunctions (2.1) is retained. The resulting predictions are compared to the ZEUS [22] and H1 [23] data in Figs.7–9. A good account of the charm structure function data can be obtained in all three models by choosing values for the charmed quark mass in the reasonable range $1.3 \leq m_c \leq 1.5$ GeV. The key question is whether one can obtain similarly accurate predictions for the J/Ψ electroproduction data using charm mass values in the same range.

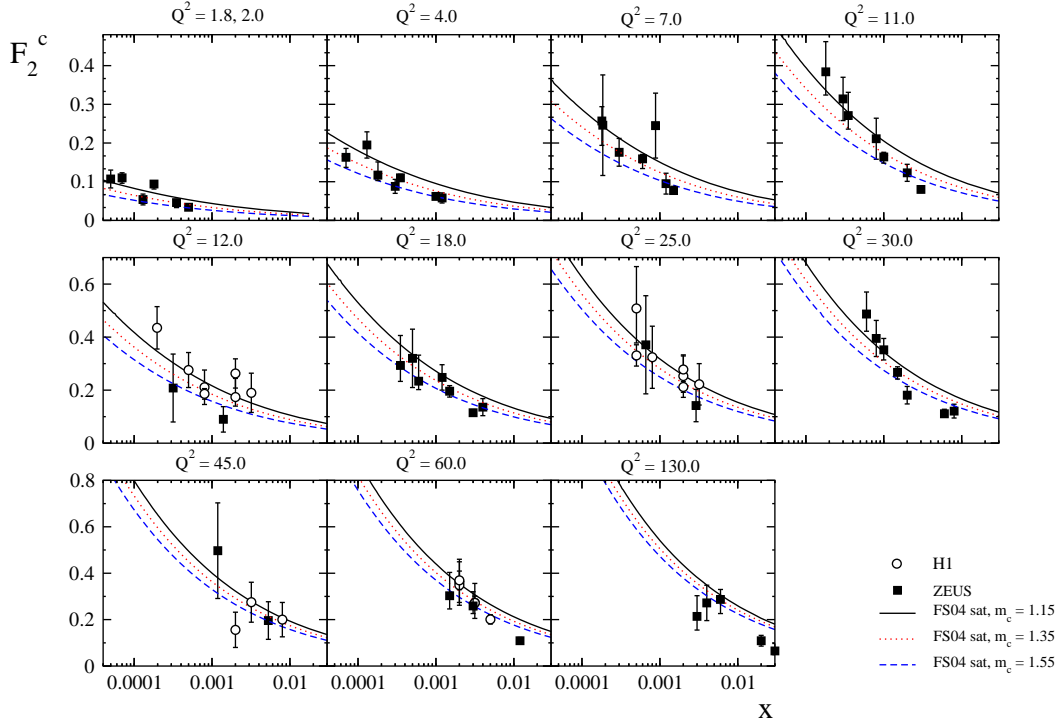


Figure 7: Comparison of the FS04 saturation model predictions for the charmed structure function F_2^c with data [22, 23].

4.2 J/Ψ wavefunctions

To calculate vector-meson production we need to know the light-cone wavefunctions of the vector mesons. Three different types of vector-meson wavefunction were studied for light mesons in [17]. For the J/Ψ we shall use wavefunctions of exactly the same functional form, but with the parameters adjusted to take into account the mass and charge of the charmed quark and the experimental value of electronic decay width of the J/Ψ -meson. In what follows, we shall comment briefly on the resulting wavefunctions, referring to [17] for detailed formulae and discussion.

In the DGKP approach [24], the r and z dependence of the scalar wavefunction is assumed to factorise into a product of gaussians. In the other two cases considered in [17], it is obtained by taking a given wavefunction in the meson rest frame. This is then boosted into a light-cone wavefunction using the Brodsky-Huang-Lepage prescription, in which the expressions for the off-shellness in the centre-of-mass and light-cone frames are equated [25] (or equivalently, the expressions for the invariant mass of the $q\bar{q}$ pair in the centre-of-mass and light-cone frames are equated [26]). In the simplest version of this approach, the wavefunction assumes a gaussian form in the meson rest frame. Alternatively NNPZ [27] have supplemented this by adding a hard “Coulomb” contribution in the hope of improving the description of the rest-frame wavefunction at small r . However there are theoretical problems with this latter wavefunction, as discussed in [17], and we shall confine

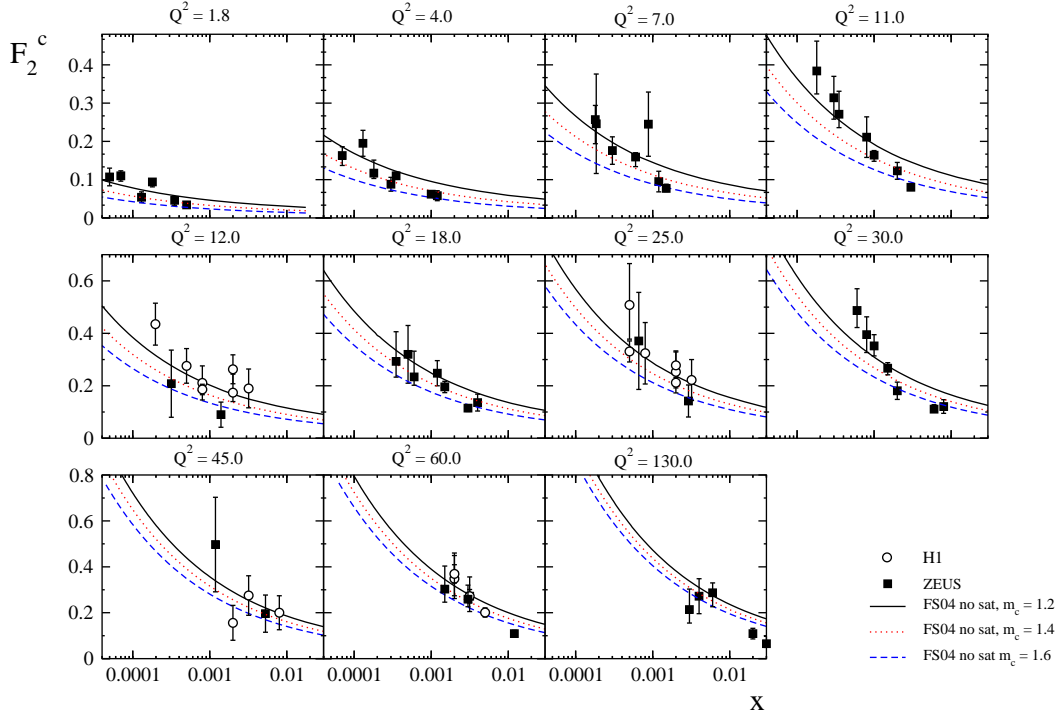


Figure 8: Comparison of the FS04 Regge predictions for the charmed structure function F_2^c with data [22, 23].

our discussion here to the DGKP and “Boosted Gaussian” wavefunctions.

The appropriate wavefunction parameters for the DGKP and Boosted Gaussian wavefunctions in the J/Ψ case are given, in the notation of [17], in Tables 1 and 2 respectively.⁴ For a charm quark of given mass, they are chosen so that the wavefunction is normalised and so that the predictions of the decay constant are consistent with the experimental value $f_{J/\Psi} = 0.273 \pm 0.005$ GeV (see [17] for further details).

DGKP parameters

m_c	ω_L	ω_T	\mathcal{N}_L	\mathcal{N}_T
1.4	0.688	0.560	18.941	8.280
1.35	0.688	0.568	18.941	8.616

Table 1: Parameters and normalisations of the DGKP light-cone wavefunctions in appropriate GeV based units.

The resulting wavefunctions are shown in Figs.10–11 for the case $m_c = 1.4$ GeV. Like the corresponding wavefunctions for the ρ and ϕ mesons (shown in [17]), the wavefunctions peak at $z = 0.5$ and $r = 0$, and go to zero as $z \rightarrow 0, 1$ and $r \rightarrow \infty$. As expected, for the J/Ψ case the peaks are much sharper. We also see that the DGKP and Boosted Gaussian

⁴Compare with Tables 2, 3 and 4 of [17].

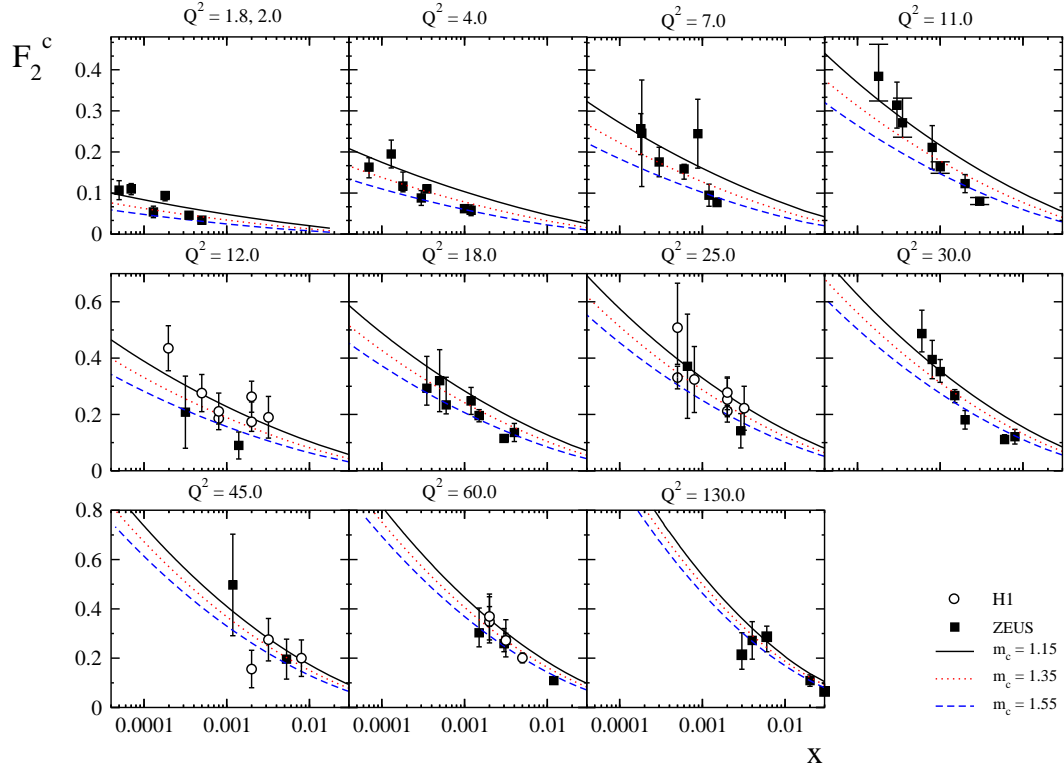


Figure 9: Comparison of the CGC model predictions for the charmed structure function F_2^c with data [22, 23].

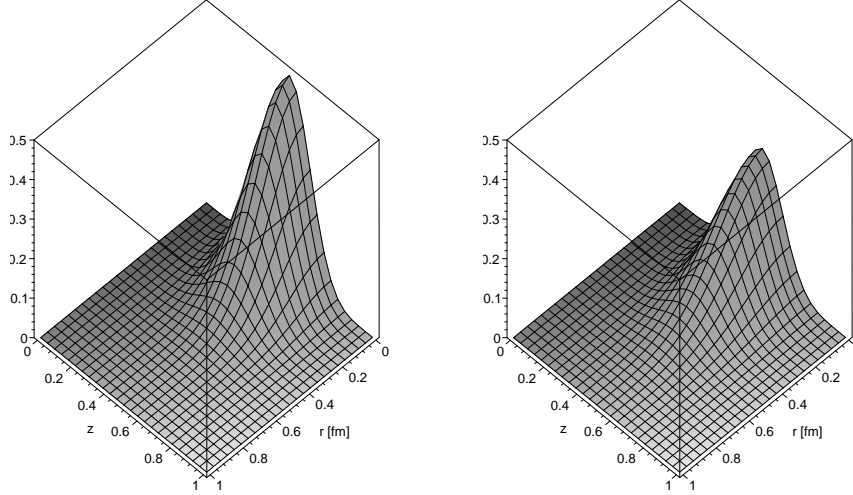


Figure 10: The J/Ψ -wavefunctions $|\Psi^L|^2$ (left) and $|\Psi^T|^2$ (right) in the DGKP model.

wavefunctions are qualitatively similar, with the transverse wavefunction having a broader distribution than the longitudinal wavefunction in each case.

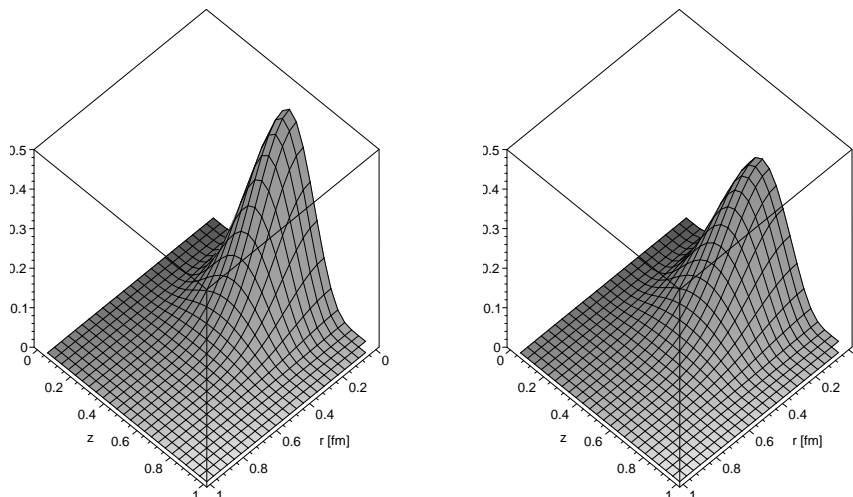


Figure 11: The J/Ψ -wavefunctions $|\Psi^L|^2$ (left) and $|\Psi^T|^2$ (right) in the Boosted Gaussian model.

Boosted Gaussian parameters

m_c	R^2	\mathcal{N}_L	\mathcal{N}_T	$f_V(L)$	$f_V(T)$
1.4	2.44	0.0363	0.0365	0.262	0.293
1.35	2.44	0.0369	0.0370	0.266	0.288

Table 2: Parameters and normalisations of the Boosted Gaussian light-cone wavefunctions in appropriate GeV based units.

4.3 J/Ψ electroproduction

Given the forms of the photon and J/Ψ wavefunctions, the cross-section in Eq.(3.4) can be calculated from Eqs.(3.2)–(3.4). However, to do this requires an estimate of the correction due to the real part in Eq.(3.3) and of the slope parameter B in Eq.(3.4).

The correction factor $(1 + \beta^2)$ for the real part of the amplitude is, as for the DVCS case, determined from the FS04 Regge model. The resulting values are illustrated in Fig.12, which shows the β^2 values obtained as functions of W at $Q^2 = 0, 10 \text{ GeV}^2$. As can be seen, the corrections from the real parts in Eq.(3.3) are a significant, but not large, correction. For the slope parameter B in Eq.(3.4) we use the simple parameterisation (in GeV units)

$$B = N \left(\frac{14.0}{(Q^2 + M_V^2)^{0.3}} + 1 \right) \quad (4.2)$$

with $N = 0.55 \text{ GeV}^{-2}$ for the J/Ψ which is in accord with the data [28, 29].

Having fixed the real parts and the slope parameter, predictions for the production cross-section can be made for both the Boosted Gaussian and DGKP wavefunctions. The charmed quark mass is adjusted within the range allowed by the charm structure function data, i.e. we use $m_c = 1.4 \text{ GeV}$ for the FS04 Regge model and $m_c = 1.35 \text{ GeV}$ for the two saturation models.

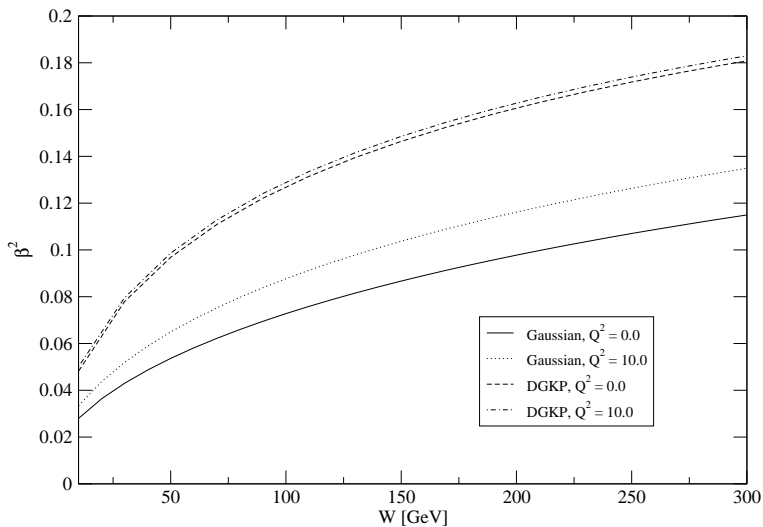


Figure 12: The W dependence of the squared ratio of the real to imaginary parts of the J/Ψ production amplitude (off transverse photons) obtained using the FS04 Regge dipole model.

The predictions for the Q^2 dependence of the total cross-section $\sigma^{\text{TOT}} = \sigma^{\text{T}} + \epsilon\sigma^{\text{L}}$ (we take $\epsilon = 0.98$) are presented in Fig.13. There is very good agreement between theory and data with relatively little dependence upon the choice of meson wavefunction.⁵ We note that for $Q^2 \lesssim 5 \text{ GeV}^2$, the predictions are very sensitive to the choice of charm quark mass. For example, the small difference between the predictions of the CGC and the other two model predictions in this region can be eliminated by fine-tuning the charm quark mass in the CGC case from 1.35 to 1.32 GeV.

The W -dependence is shown for a range of Q^2 values in Figs.14–15. As before, agreement is good and there is little dependence on the choice of meson wavefunction. Large differences between the models only arise at energies beyond the current experimental range ($W \gtrsim 400 \text{ GeV}$), but again the differences between the two saturation models can be significantly reduced by fine-tuning the chosen values for the charmed quark mass, especially at low Q^2 .

Finally, our predictions for the Q^2 dependence of the cross-section ratio $R = \sigma_L/\sigma_T$ at $W = 90 \text{ GeV}$ are shown in Fig.16. There is once again good agreement between theory and data with slightly more dependence upon the choice of meson wavefunction. Note that the longitudinal-to-transverse ratio R increases approximately linearly with Q^2 and, in contrast to the ρ and ϕ cases [17], does not flatten out in the currently accessible range of Q^2 . This is to be expected, since in the extreme non-relativistic limit the wavefunction approaches a delta function whence the ratio $R \propto Q^2/m_c^2$ for all Q^2 .

⁵Unlike the case for the light mesons [17].

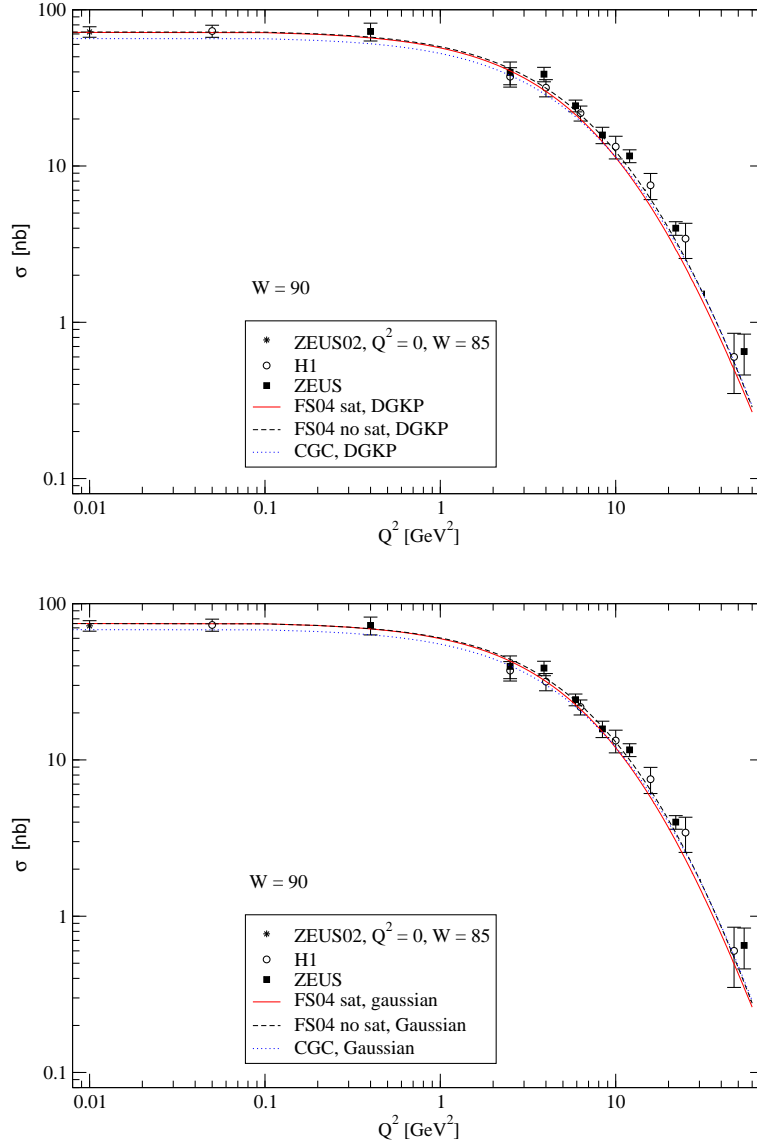


Figure 13: Comparison of the model predictions to the data [28, 29] for exclusive J/Ψ meson production: Q^2 dependence. Upper plot: DGKP wavefunction. Lower plot: Boosted Gaussian wavefunction.

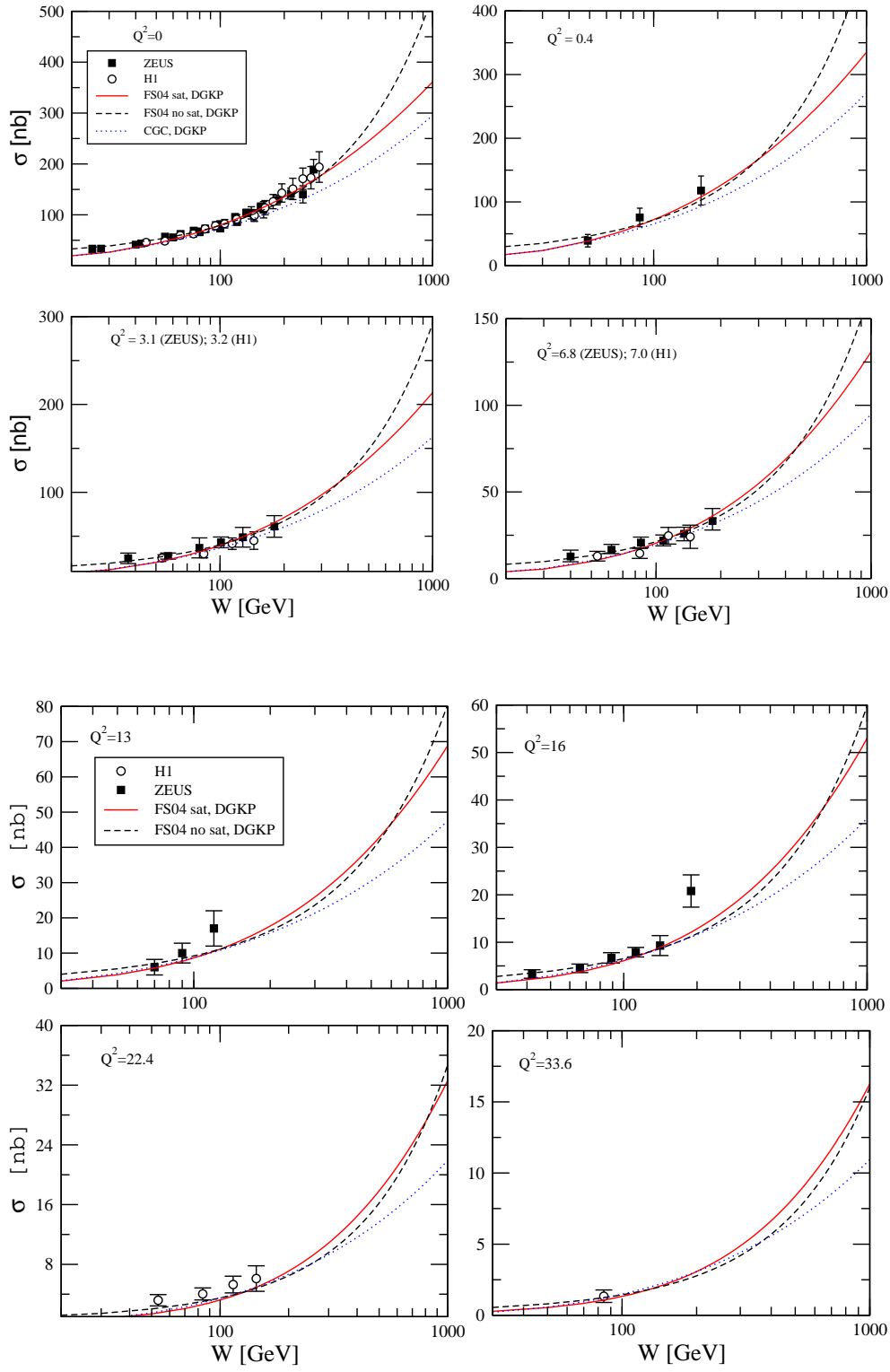


Figure 14: Comparison of the model predictions to the data [28, 29] for exclusive J/Ψ meson production using the DGKP meson wavefunction: W dependence.

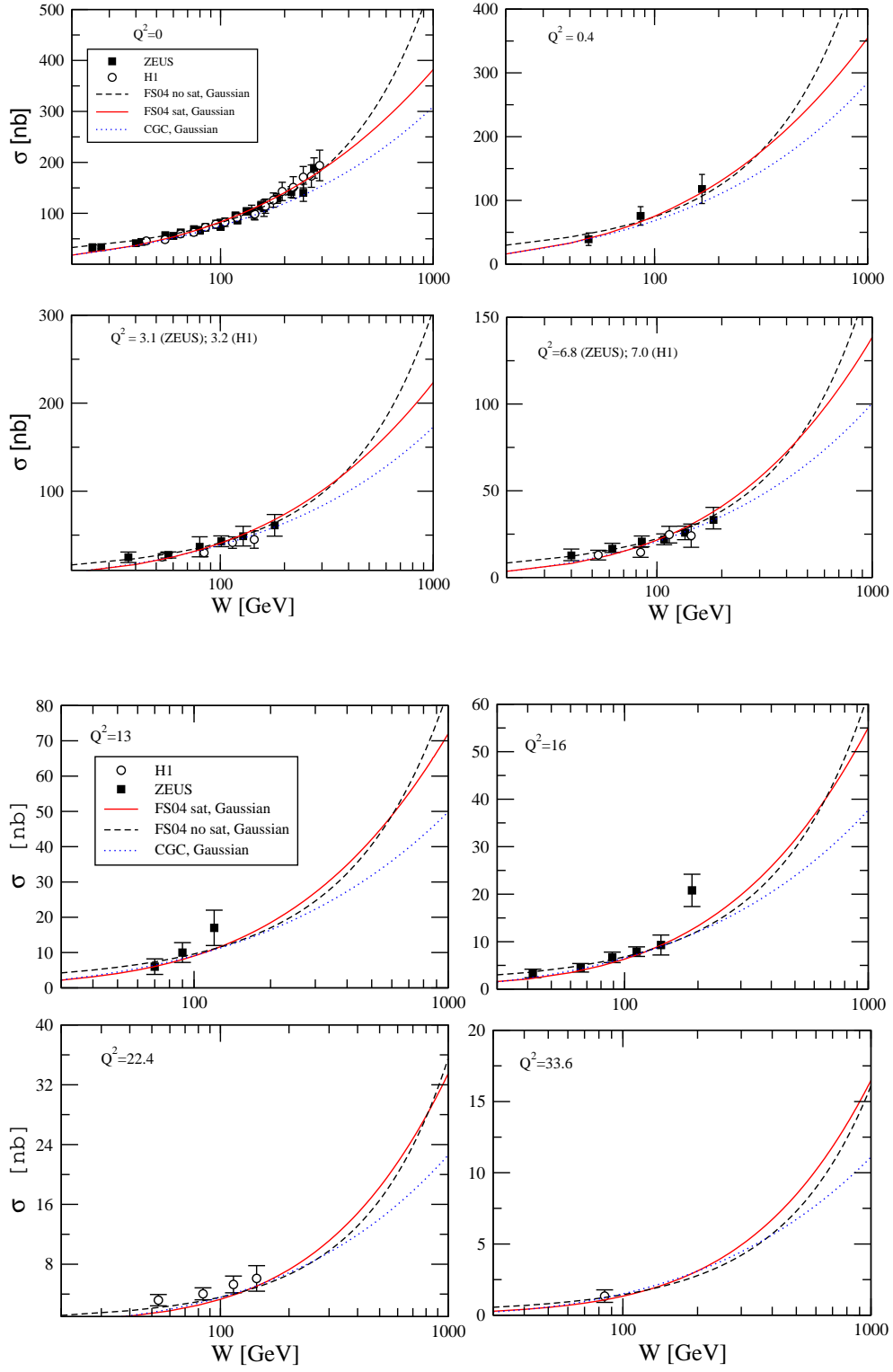


Figure 15: Comparison of the model predictions to the data [28, 29] for exclusive J/Ψ meson production using the Boosted Gaussian meson wavefunction: W dependence.

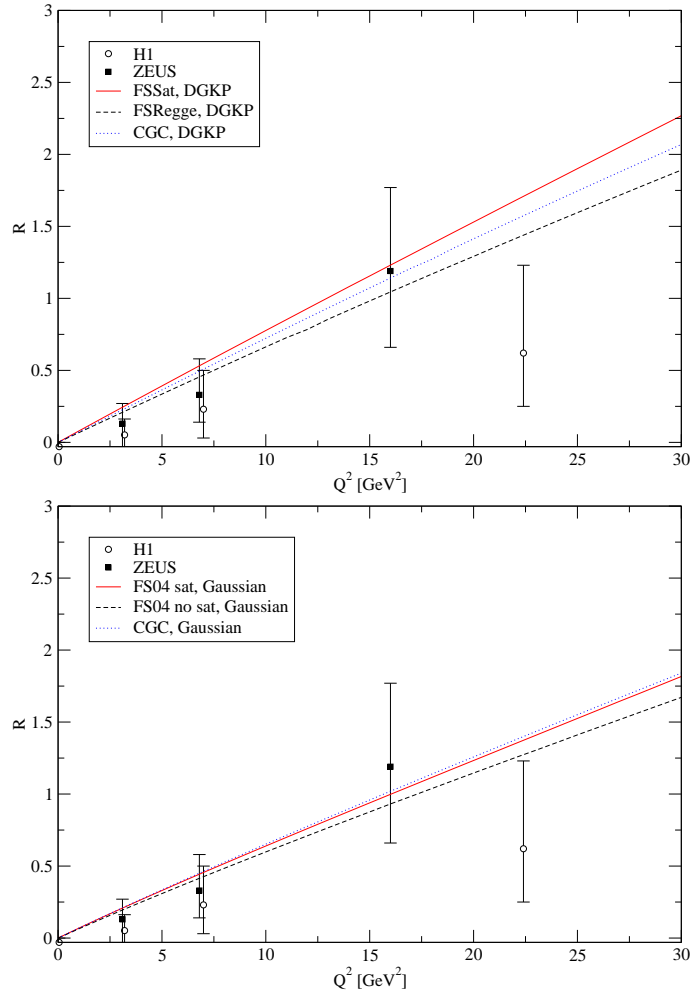


Figure 16: Comparison of the model predictions to the data [28, 29] on the ratio R for exclusive J/Ψ meson.

5. Diffractive deep inelastic scattering (DDIS)

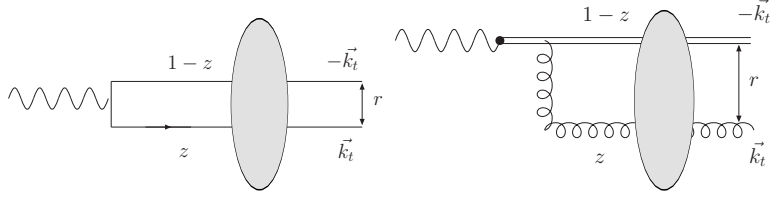


Figure 17: The $q\bar{q}$ and qqg contributions to $F_2^{D(3)}$.

To conclude our study we turn to the diffractive deep inelastic scattering (DDIS) process

$$\gamma^* + p \rightarrow X + p \quad ,$$

where the hadronic state X is separated from the proton by a rapidity gap. In this process, in addition to the usual variables x and Q^2 there is a third variable M_X^2 . In practice, x and M_X^2 are often replaced by the variables $x_{\mathcal{P}}$ and β :

$$x_{\mathcal{P}} \simeq \frac{M_X^2 + Q^2}{W^2 + Q^2} \quad \beta = \frac{x}{x_{\mathcal{P}}} \simeq \frac{Q^2}{M_X^2 + Q^2} \quad . \quad (5.1)$$

In the diffractive limit $s \gg Q^2, m_X^2$ and so $x_{\mathcal{P}} \ll 1$.

In the dipole model, the contribution due to quark-antiquark dipoles to the structure function $F_2^{D(3)}$ can be obtained from a momentum space treatment as described in [30, 7]. However, if we are to confront the data at low values of β , corresponding to large invariant masses M_X , it is necessary also to include a contribution from the higher Fock state qqg . We can estimate this contribution using an effective “two-gluon dipole” approximation due to Wüsthoff [30], as illustrated in Fig.17.

Again, the predictions obtained in this way involve no adjustment of the dipole cross-sections and photon wavefunctions used to describe the F_2 data. We are however free to adjust the forward slope for inclusive diffraction (B) within the range acceptable to experiment, which means that the overall normalisation, but not the energy dependence, of $F_2^{D(3)}$ is free to vary somewhat. We take $B = 6.8 \text{ GeV}^{-2}$ when making our CGC and FS04 saturation predictions and $B = 8.0 \text{ GeV}^{-2}$ when making the FS04 Regge predictions. Note that a value of 8.0 GeV^{-2} is rather high compared to the $\approx 6 \text{ GeV}^{-2}$ favoured by the H1 FPS data [31] although it is in the range allowed by the ZEUS LPS data [32]. The need for a larger value of B for the FS04 Regge model arises since the corresponding dipole cross-section is significantly larger than the FS04 saturation model at large values of r and this enhancement is magnified in inclusive diffraction since it is sensitive to the square of the dipole cross-section. We should also bear in mind that the tagged proton data are subject to an overall $\approx 10\%$ normalisation uncertainty. We are also somewhat free to vary the value of α_s used to define the normalisation of the model dependent qqg component, which is important at low values of β . Rather arbitrarily we take $\alpha_s = 0.1$ and take the view that the theory curves are less certain in the low β region.

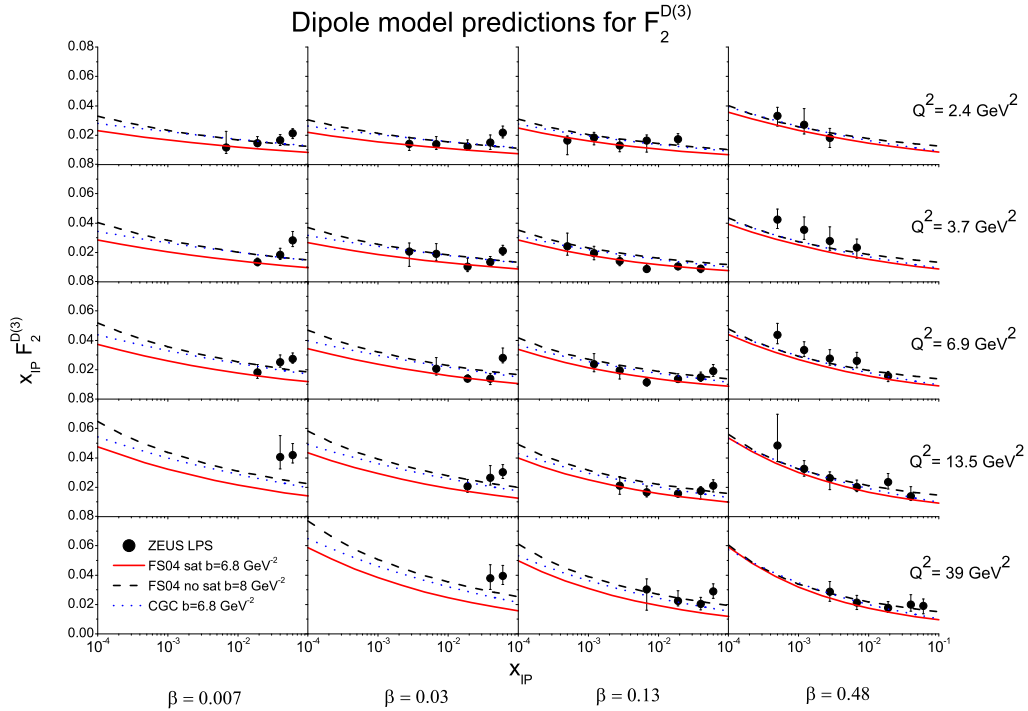


Figure 18: Model predictions compared to the ZEUS LPS data [32].

In Fig.18 we compare the recent ZEUS LPS data [32] on the $x_{\mathcal{P}}$ dependence of the structure function $F_2^{D(3)}$ at various fixed Q^2 and β with the models⁶. The agreement is good except at the larger $x_{\mathcal{P}}$ values. Indeed, the χ^2 values per data point are very close to unity for all three models for $x_{\mathcal{P}} < 0.01$. Disagreement at larger $x_{\mathcal{P}}$ is to be expected since this is the region where we anticipate a significant non-diffractive contribution which is absent in the dipole model prediction. Note that the three models produce similar predictions at larger values of β .

Contamination from secondary exchanges is avoided in the FPC data [34], in which the non-diffractive contribution is explicitly removed by the ZEUS method of analysis. However this comes at the cost of including proton dissociation contributions, since the mass of the target fragments (M_Y) is only limited to being below 2.3 GeV. The predictions of our three models are compared with these data in Fig.19 and Fig.20, where the theory curves have been divided by 0.7 to allow for proton dissociation contributions, assumed to be a fixed fraction of the total, independent of the kinematic variables. This is obviously a crude approximation but it is supported by the experimental analyses. These data suggest that the CGC and Regge model predictions are perhaps overshooting the data at low β whilst the three models produce very similar predictions at larger values of β , i.e. $\beta \gtrsim 0.4$.

⁶Predictions for the original Iancu et al CGC model have previously been published in [33].

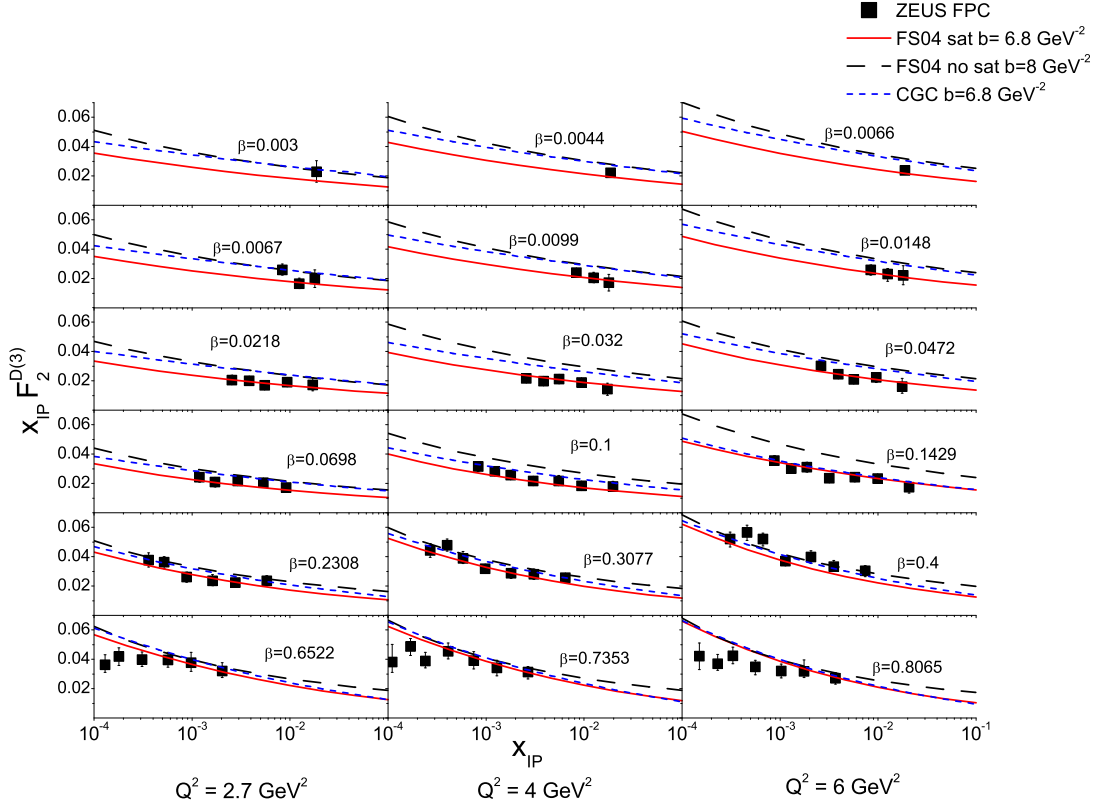


Figure 19: Model predictions compared to the ZEUS FPC data with $M_Y < 2.3$ GeV (low Q^2) [34].

Specifically, for the FS04 saturation model $\chi^2 = 238$ for the entire 156 data points whilst the CGC and FS04 Regge models have $\chi^2 = 147$ and 150 respectively for the 94 data points with $\beta > 0.3$. However, we must be careful not to overinterpret the data. The low β region is precisely the region where there is an appreciable $q\bar{q}g$ component which is subject to a rather large theoretical uncertainty. Moreover, we must not forget that (for the FPC data) we have assumed that the fraction of events which contain a dissociated proton is constant. Recall also that there is an uncertainty in the value of the forward slope parameter used in determining the theoretical predictions.

Comparison to the H1 data with tagged protons [31] is to be found in Fig.21 and Fig.22. The story is similar to that for the ZEUS data and the evidence for an overshoot of the CGC and Regge model predictions at low β is strengthened. The $Q^2 = 2.7$ GeV² panes in Fig.22 illustrate this point the best. Again, we should not interpret this as evidence against these dipole models due to the uncertainty in the $q\bar{q}g$ contribution in the low β region. The agreement between all models and the data at larger values of β and low

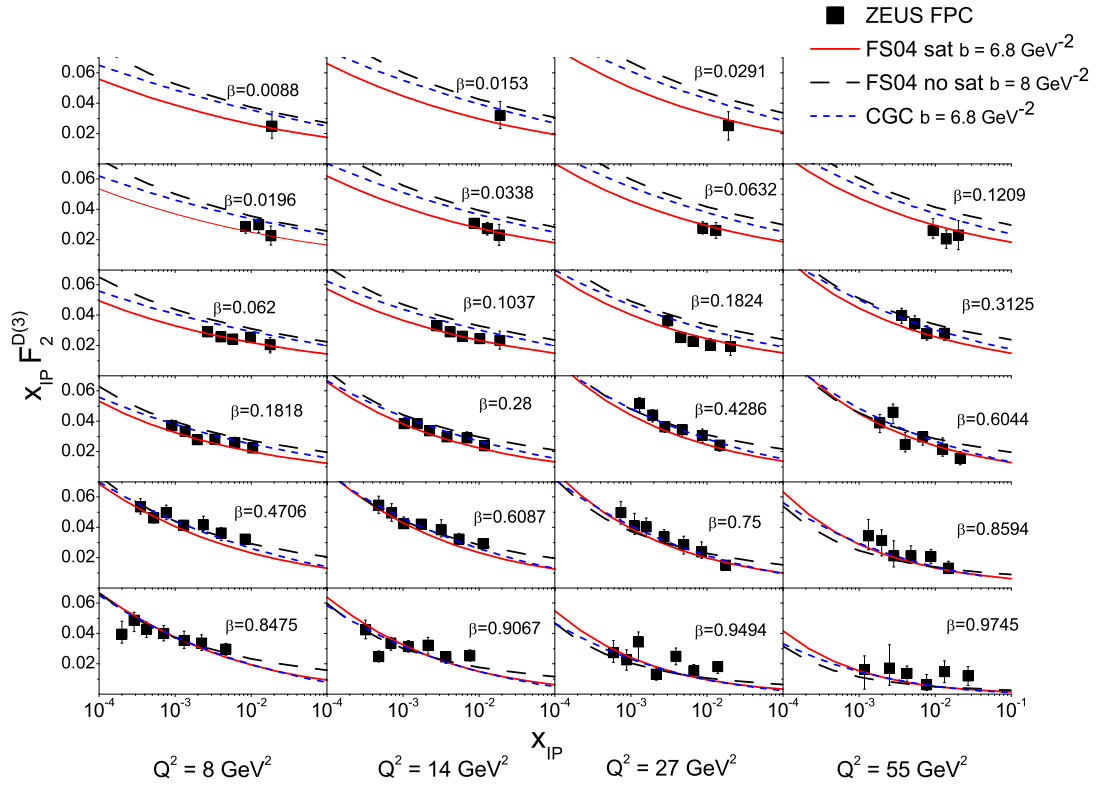


Figure 20: Model predictions compared to the ZEUS FPC data with $M_Y < 2.3$ GeV (high Q^2) [34].

enough $x_{\mathbb{P}}$ is satisfactory.⁷

In Figs.23–26 we compare to the H1 data collected with some proton dissociation, i.e. $M_Y < 1.6$ GeV [35], and in order to include the effect of proton dissociation we now divide the theory by a factor 0.8. The FS04 saturation model performs well over the whole kinematic region with $x_{\mathbb{P}} \lesssim 10^{-2}$ whilst once again the CGC and Regge models overshoot the data at low β . On these plots we also show the result of computing $F_2^{D(3)}$ without including the $q\bar{q}g$ component: clearly the data require an additional contribution at low β . We note that it is possible to improve the quality of the agreement between data and theory if we are allowed to increase the fraction of proton dissociation assumed in the data (there is perhaps a hint that this increase should also be slightly larger at higher values of Q^2). For example, for the 170 data points in Fig.26 with $\beta \geq 0.4$ and $x_{\mathbb{P}} < 0.01$ we find χ^2 values of 244, 330 and 263 for the FS04 saturation, FS04 Regge and CGC models respectively if we globally decrease the scaling factor from 0.8 to 0.7.

⁷The FS04 saturation fit has $\chi^2 = 37$ for the 40 points with $x_{\mathbb{P}} < 0.01$ whilst the CGC and FS04 Regge fits both have χ^2 per data point below 2 for the 18 points with $\beta \geq 0.35$.

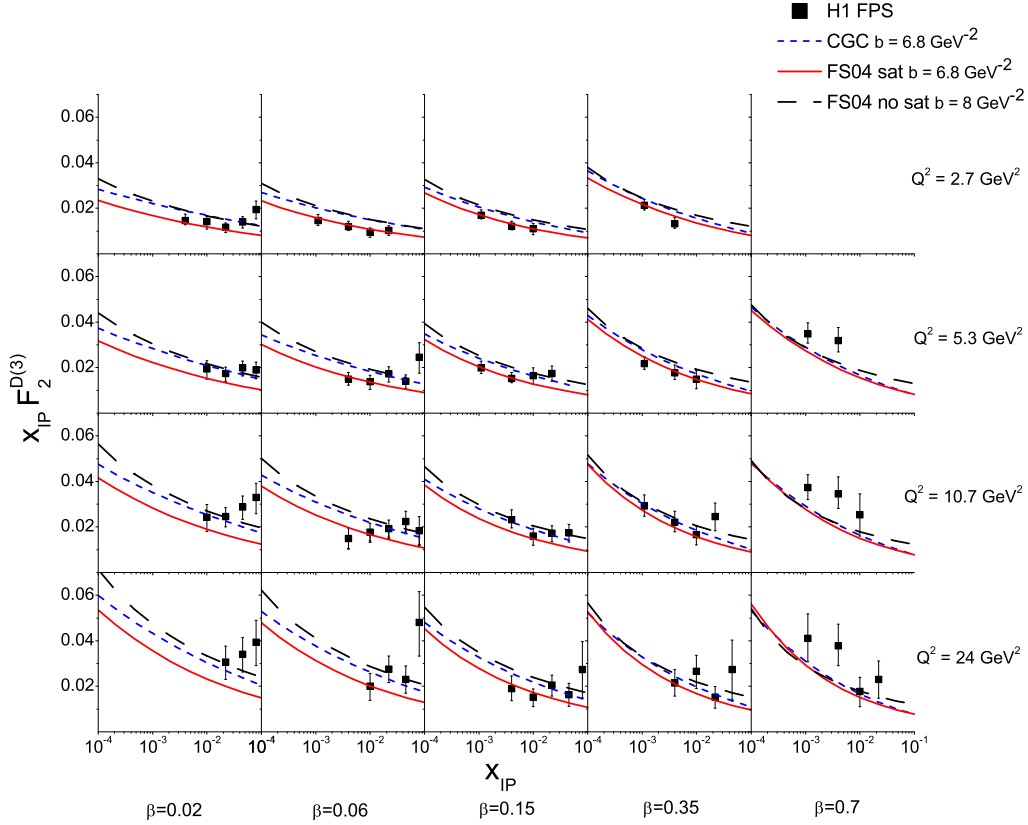


Figure 21: Model predictions compared to the H1 FPS data: x_{IP} dependence [31].

Before leaving the H1 data we should say that, strictly speaking, all of the H1 data refer to the reduced diffractive cross-section, $\sigma_r^{D(3)}$. However the difference between that quantity and the diffractive structure function $F_2^{D(3)}$ is mostly negligible and is never more than 10%.

In summary, the DDIS data at large enough $\beta \gtrsim 0.4$ and small enough $x_{IP} \lesssim 0.01$ are consistent with the predictions of all three dipole models. However the data themselves would have a much greater power to discriminate between models if the forward slope parameter were measured to better accuracy. At smaller values of β , the data clearly reveal the presence of higher mass diffractive states which can be estimated via the inclusion of a $q\bar{q}g$ component in the dipole model calculation under the assumption that the three-parton system interacts as a single dipole according to the universal dipole cross-section. The theoretical calculation at low β must be improved before the data in the region can be utilised to disentangle the physics of the dipole cross-section. Nevertheless, it is re-assuring to observe the broad agreement between theory and data in the low β region.

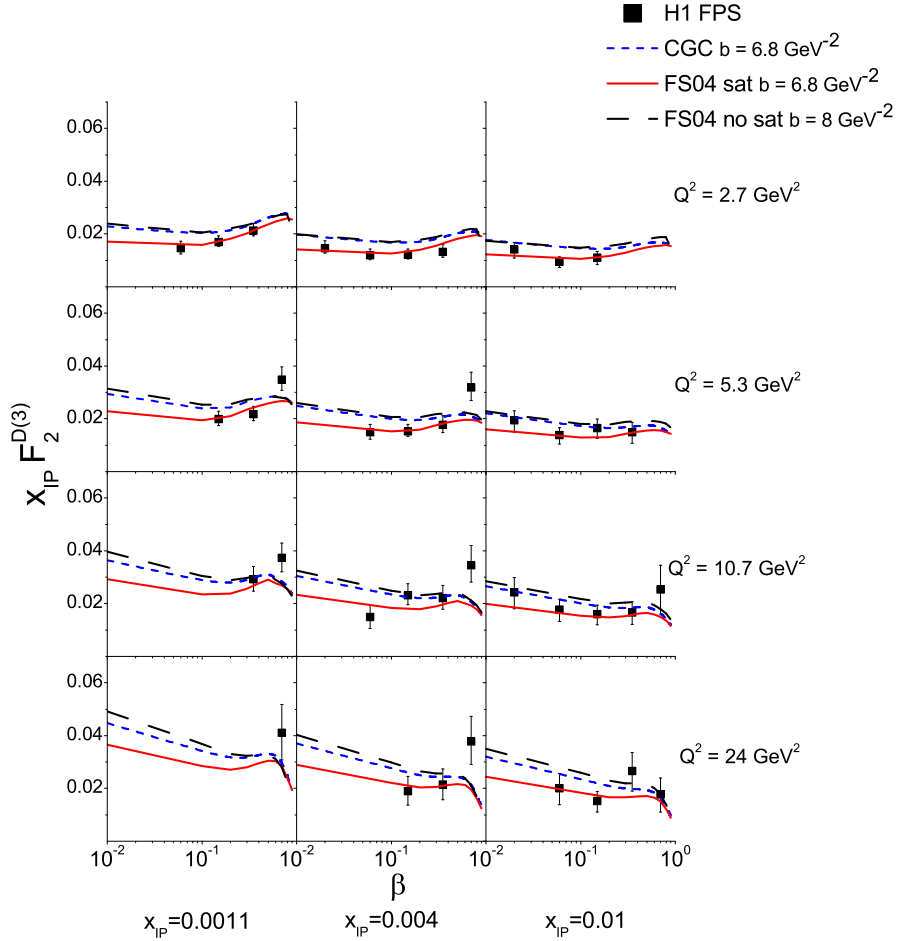


Figure 22: Model predictions compared to the H1 FPS data: β dependence [31].

6. Conclusion

The dipole scattering approach, when applied to diffractive electroproduction processes, clearly works very well indeed. The HERA data now constitute a large body of data which is typically accurate to the 10% level or better, and without exception the dipole model is able to explain the data in terms of a single universal dipole scattering cross-section. Perhaps the most important question to ask of the data is the extent to which saturation dynamics is present. Although the F_2 data suggest the presence of saturation dynamics [9], the remaining data on exclusive processes and on $F_2^{D(3)}$ are unable to distinguish between the models we consider here: these data are therefore unable to offer additional information on the possible role of saturation. We do note that a more accurate determination of the forward slope parameter in diffractive photo/electro-production processes would sig-

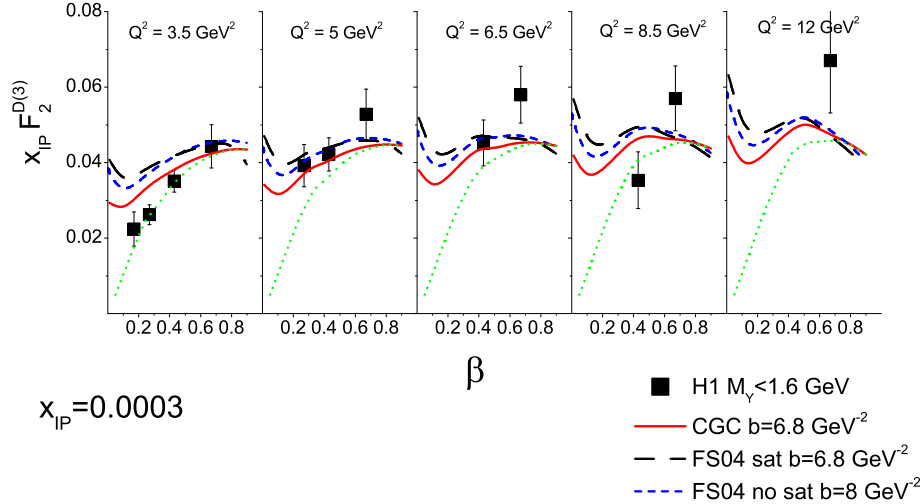


Figure 23: Model predictions compared to the H1 data with $M_Y < 1.6$ GeV [35]: β dependence at $x_P = 0.0003$. Green dotted curve shows the contribution without including the $q\bar{q}g$ component.

nificantly enhance the impact of the data. However, it is hard to avoid the conclusion that only with more precise data or with data out to larger values of the centre-of-mass energy will we have the chance to make a definitive statement on the role of saturation without the inclusion of the low Q^2 $F_2(x, Q^2)$ data in the analysis.

Acknowledgments

This research was supported in part by the UK's Particle Physics and Astronomy Research Council. We should like to thank Paul Laycock and Paul Newman for helpful discussions.

References

- [1] N.N. Nikolaev and B.G. Zakharov, Z. Phys. **C49** (1991) 607; **C53** (1992) 331.
- [2] A.H. Mueller, Nucl. Phys. **B415** (1994) 273; A.H. Mueller and B. Patel, Nucl. Phys. **B425** (1994) 471.
- [3] J.R. Forshaw, G. Kerley and G. Shaw, Phys. Rev. **D60** (1999) 074012; Nucl. Phys. **A675** (2000) 80.
- [4] H. Fraas, B. J. Read and D. Schildknecht, Nucl. Phys. **B86** (1975) 346.
- [5] G. Shaw, Phys. Rev. **D47** (1993) R3676; G. Shaw, Phys. Lett. **B228** (1989) 125; P. Ditsas and G. Shaw, Nucl. Phys. **B113** (1976) 246.
- [6] L. Frankfurt, V. Guzey and M. Strikman, Phys. Rev. **D58** (1998) 094039.
- [7] K. Golec-Biernat and M. Wüsthoff, Phys. Rev. **D59** (1999) 014017; Phys. Rev. **D60** (1999) 114023.

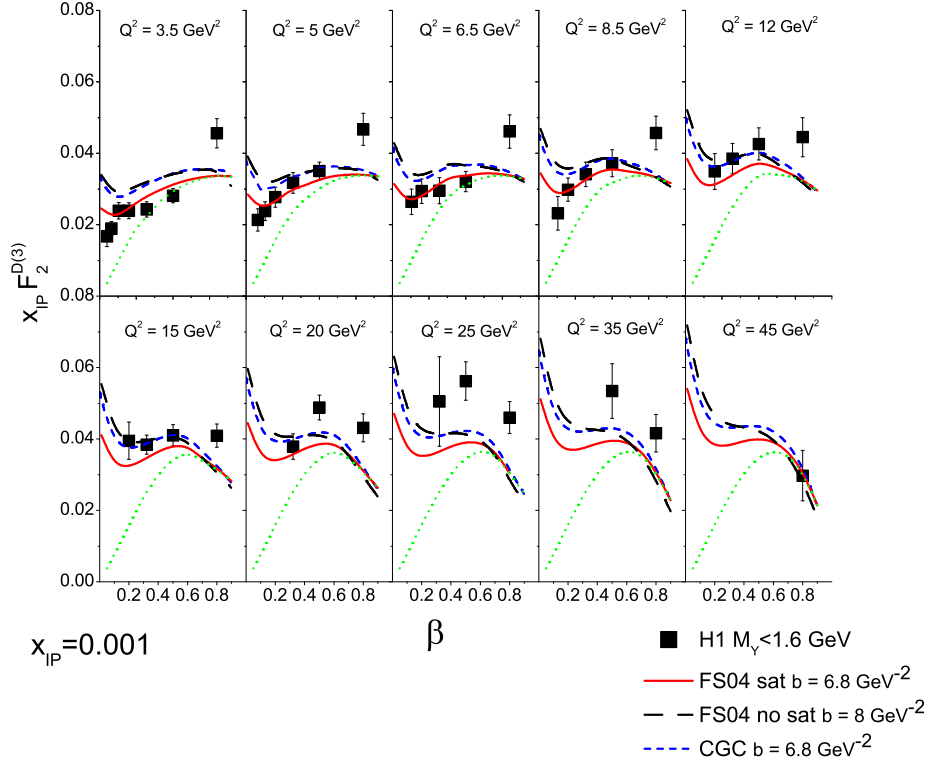


Figure 24: Model predictions compared to the H1 data with $M_Y < 1.6$ GeV [35]: β dependence at $x_P = 0.001$. Green dotted curve shows the contribution without including the $q\bar{q}$ component.

- [8] J.R. Forshaw and G. Shaw, “Colour dipoles and diffraction” in “Hadrons and their electromagnetic Interactions”, editors F. Close, A. Donnachie and G. Shaw, C.U.P.(in press).
- [9] J.R. Forshaw and G. Shaw *JHEP* **0412** (2004) 052.
- [10] D.O. Caldwell et al, *Phys. Rev. Lett.* **40** (1978) 1222.
- [11] M. McDermott, L. Frankfurt, V. Guzey and M. Strikman, *Eur. Phys. J.* **C16** (2000) 641.
- [12] E. Iancu, K. Itakura and S. Munier, *Phys. Lett.* **B590** (2004) 199.
- [13] H. Kowalski, L. Motyka and G. Watt, arXiv:hep-ph/0606272.
- [14] S. Chekanov et al, ZEUS Collab., *Eur. Phys. J.* **C21** (2001) 442.
- [15] C. Adloff et al, H1 Collab., *Eur. Phys. J.* **C21** (2001) 33.
- [16] H. Kowalski and D. Teaney, *Phys. Rev.* **D68** (2003) 114005.
- [17] J. R. Forshaw, R. Sandapen and G. Shaw, *Phys. Rev.* **D69** (2004) 094013.
- [18] M. Kuroda and D. Schildknecht, *Eur. Phys. J.* **C37** (2004) 205; *Phys. Lett.* **B638** (2006) 473.
- [19] M.F. McDermott, R. Sandapen and G. Shaw, *Eur. Phys. J.* **C22** (2002) 665.

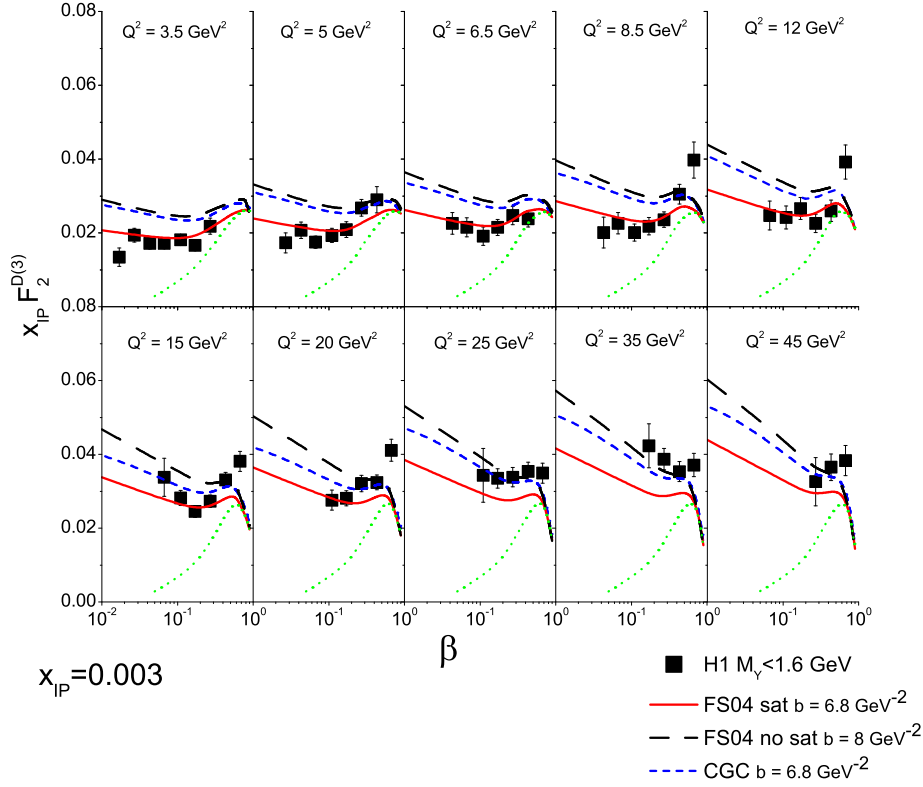


Figure 25: Model predictions compared to the H1 data with $M_Y < 1.6$ GeV [35]: β dependence at $x_P = 0.003$. Green dotted curve shows the contribution without including the $q\bar{q}g$ component.

- [20] A. Aktas et al, H1 Collab., Eur. Phys. **C44** (2005) 1.
- [21] S. Chekanov et al, ZEUS Collab., Phys. Lett. **B573** (2003) 46.
- [22] J. Breitweg et al, ZEUS Collab., Phys. Lett. **B407** (1997) 402; Eur. Phys. J. **C12** (2000) 35; Eur. Phys. J. **C16** (2000) 181; S. Chekanov et al, ZEUS Collab., Phys. Rev. **D69** (2004) 012004.
- [23] C. Adloff et al, H1 Collab., Z. Phys. **C72** (1996) 503; Phys. Lett. **B528** (2002) 199; A. Aktas et al, H1 Collab., Eur. Phys. J. **C45** (2006) 23.
- [24] H. G. Dosch, T. Gousset, G. Kulzinger and H. J. Pirner, Phys. Rev. **D55** (1997) 2602.
- [25] S. J. Brodsky, T. Huang and G. P. Lepage, SLAC-PUB-2540 (1980). Shorter version contributed to 20th Int. Conf. on High Energy Physics, Madison, Wisc., Jul 17-23, 1980.
- [26] A. Donnachie, J. Gravelis and G. Shaw, Phys. Rev. **D63** (2001) 114013.
- [27] J. Nemchik, N. N. Nikolaev, E. Predazzi and B. G. Zakharov, Z. Phys. **C75** (1997) 71.
- [28] S. Aid et al, H1 Collab., Nucl. Phys. **B468** (1996) 3; Nucl. Phys. **B472** (1996) 3; C. Adloff et al., H1 Collab., Phys. Lett. **B483** (2000) 23; A. Aktas et al., H1 Collab., Eur. Phys. J. **C46** (2006) 585.

- [29] S. Chekanov et al., ZEUS Collab., Eur. Phys. J. **C24** (2002) 345; Nucl. Phys. **B695** (2004) 3.
- [30] M. Wüsthoff, Phys. Rev. **D56** (1997) 4311.
- [31] A. Aktas et al, H1 Collab., “Diffractive deep-inelastic scattering with a leading proton at HERA”, DESY-06-048, arXiv:hep-ex/0606003.
- [32] S. Chekanov et al, ZEUS Collab., Eur. Phys. J. **C38** (2004) 43.
- [33] J.R. Forshaw, R. Sandapen and G. Shaw, Phys. Lett. **B594** (2004) 283.
- [34] S. Chekanov et al, ZEUS Collab., Nucl. Phys. **B713** (2005) 3.
- [35] A. Aktas et al, H1. Collab., “Measurement and QCD analysis of the diffractive deep-inelastic scattering cross section at HERA”, DESY-06-049, arXiv:hep-ex/0606004.

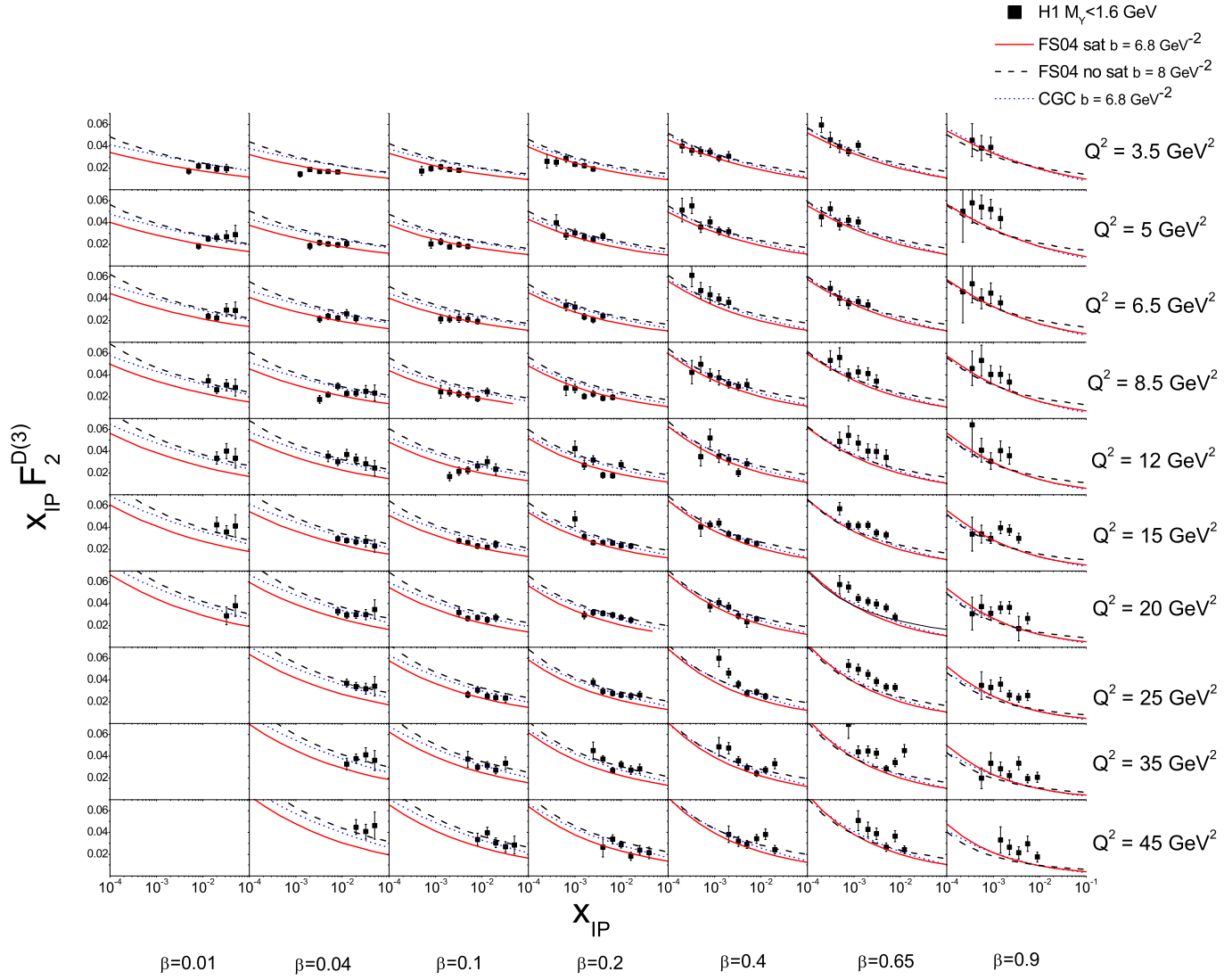


Figure 26: Model predictions compared to the H1 data with $M_Y < 1.6$ GeV [35]: x_P dependence.